Application of Optical Instrumentation in Medicine XIII

Medical Image Production, Processing, and Display

Roger H. Schneider, Samuel J. Dwyer III
Chairmen/Editors

Proceedings of SPIE—The International Society for Optical Engineering

Volume 535

Application of Optical Instrumentation in Medicine XIII

Medical Image Production, Processing, and Display

Roger H. Schneider, Samuel J. Dwyer III
Chairmen/Editors

Cooperating Organizations
Center for Devices and Radiological Health, FDA
The Society of Radiological Engineers
IEEE Computer Society, Technical Committee on Computational Medicine

February 3-6, 1985
Newport Beach, California

Published by
SPIE—The International Society for Optical Engineering
P.O. Box 10, Bellingham, Washington 98227-0010 USA
Telephone 206/676-3290 (Pacific Time) • Telex 46-7053

The papers appearing in this book comprise the proceedings of the meeting mentioned on the cover and title page. They reflect the authors' opinions and are published as presented and without change, in the interests of timely dissemination. Their inclusion in this publication does not necessarily constitute endorsement by the editors or by SPIE.

Please use the following format to cite material from this book:
Author(s), "Title of Paper," *Application of Optical Instrumentation in Medicine XIII: Medical Image Production, Processing, and Display,* Roger H. Schneider, Samuel J. Dwyer III, Editors, Proc. SPIE 535, page numbers (1985).

Library of Congress Catalog Card No. 74-169214
ISBN 0-89252-570-3

Printed in the United States of America.

APPLICATION OF OPTICAL INSTRUMENTATION IN MEDICINE XIII
MEDICAL IMAGE PRODUCTION, PROCESSING, AND DISPLAY

Volume 535

Conference Committee

Chairmen

Roger H. Schneider, Center for Devices and Radiological Health, FDA
Samuel J. Dwyer III, University of Kansas, College of Health Sciences and Hospital

Program Committee

Roger Bauman, Massachusetts General Hospital & Harvard Medical School; **Stuart I. Brown,** University Hospital, University of California/San Diego; **Arthur Burgess,** University of British Columbia, Health Sciences Center Hospital, Canada; **Kunio Doi,** Kurt Rossman Laboratories for Radiological Image Research/University of Chicago; **Andre J. Duerinckx,** University of Miami School of Medicine; **Melvin M. Figley,** University of Washington; **Kenneth M. Hanson,** Los Alamos National Laboratory; **Steven C. Horii,** New York University Medical Center; **H. K. Huang,** University of California/Los Angeles; **Robert J. Jennings,** Center for Devices and Radiological Health, FDA; **James L. Lehr,** University of Chicago; **Murray Loew,** George Washington University; **Albert Macovski,** Stanford University Medical Center; **Judith M. S. Prewitt,** AT&T Bell Laboratories; **Rodney Shaw,** Eastman Kodak Company; **Stephen W. Smith,** Center for Devices and Radiological Health, FDA; **Michel M. Ter-Pogossian,** Washington University School of Medicine; **Robert F. Wagner,** Center for Devices and Radiological Health, FDA

Session Chairmen

Session 1 —Image Statistics & Perception: I, **Kunio Doi,** Kurt Rossman Laboratories for Radiological Image Research/University of Chicago
Session 2 —Image Statistics & Perception: II, **Robert F. Wagner,** Center for Devices and Radiological Health, FDA
Session 3 —Image Statistics & Perception: III, **Arthur Burgess,** University of British Columbia, Health Sciences Center Hospital, Canada
Session 4 —Computing Images From Data, **Kenneth M. Hanson,** Los Alamos National Laboratory
Session 5 —Detector Physics I: Scatter, **H. K. Huang,** University of California/Los Angeles
Session 6 —Detector Physics II: Film Screen Systems, **Rodney Shaw,** Eastman Kodak Company; **Robert J. Jennings,** Center for Devices and Radiological Health, FDA
Session 7 —Detector Physics III: Digital, **Albert Macovski,** Stanford University Medical Center
Session 8 —Detector Physics IV: Semiconductors & Photoconductors, **Roger Schneider,** Center for Devices and Radiological Health, FDA
Session 9 —Detector Physics V: Ultrasound & NMR, **Stephen W. Smith,** Center for Devices and Radiological Health, FDA
Session 10—Photography, **Stuart I. Brown,** University Hospital, University of California/San Diego
Session 11—Image Processing I: General, **James L. Lehr,** University of Chicago
Session 12—Image Processing II A: Task Oriented—Cranial, **Murray Loew,** George Washington University
Session 13—Image Processing II B: Task Oriented—Chest, **Gordon Johnson,** Center for Devices and Radiological Health, FDA
Session 14—Image Processing II C: Task Oriented—Gastro Intestinal, **Steven C. Horii,** New York University Medical Center

APPLICATION OF OPTICAL INSTRUMENTATION IN MEDICINE XIII
MEDICAL IMAGE PRODUCTION, PROCESSING, AND DISPLAY

Volume 535

INTRODUCTION

This was the thirteenth meeting of this series. While this did not arouse any supertitious fears among the chairmen or program committee we were wondering whether it would attain the high standard set by its immediate predecessor. We need not have worried. The format and forum of this meeting seem to resonate well with the interests and needs of the medical imaging community in this era. The response to the call for papers was outstanding. By all accounts the standard was met and surpassed.

The entire first day of the meeting dealt with statistical and information theory approaches to image formation and visual perception—the conveyance of information to human observers through imaging channels. These three sessions contain an excellent presentation of the state of the art in this exciting field. It is clear that the formalism is maturing and can be considered almost complete at some basic level. It is also clear that the tantalizing goal of predicting decision-maker performance in complex milieu is yet beyond our grasp. The system formulation is proceeding enthusiastically but the value of the observer's subjective opinion must still be acknowledged.

On the second day, Sesson 4 presented several new clinical applications of image reconstruction and Session 5 presented theoretical and experimental characterizations of scatter and corrective methods. Session 6 was an outstanding and comprehensive updating of our understanding of screen intensified film systems with seven excellent papers from our colleagues in that industry. The scope and depth of treatment of this topic in this session were unique for any single meeting in my experience. These authors are to be congratulated!

The third day presented new information on the physics and applications of semiconductor and photoconductor x-ray detectors, ultrasound, and NMR imaging. In addition, medical photographic applications were discussed and the topic of image processing was introduced with five papers on hardware and software techniques for more or less general use.

The fourth day presented clinical applications of image processing for CT and conventional x-ray images of the head, chest, and gastro-intestinal areas and ended with a PACS workshop to prepare us for the next two days to come. The PACS papers are published in a companion volume of these proceedings.

We had some reservations that a six-day meeting could prove too strenuous for organizers and attendees alike. Upon reflection from the vantage of a two-month respite, it was a large and concentrated dose of new and important information and a valuable and enjoyable experience. The enthusiasm of all was sustained throughout.

Roger H. Schneider
Center for Devices and Radiological Health, FDA

APPLICATION OF OPTICAL INSTRUMENTATION IN MEDICINE XIII
MEDICAL IMAGE PRODUCTION, PROCESSING, AND DISPLAY

Volume 535

Contents

APPLICATION OF OPTICAL INSTRUMENTATION IN MEDICINE XIII
MEDICAL IMAGE PRODUCTION, PROCESSING, AND DISPLAY

Volume 535

Session 1

Image Statistics & Perception: I

Chairman
Kunio Doi
Kurt Rossman Laboratories for Radiological Image Research/University of Chicago

Digital image processing: optimal spatial filter for maximization of the perceived SNR based on a statistical decision theory model for the human observer

Heang-Ping Chan, Charles E. Metz, and Kunio Doi

Kurt Rossmann Laboratories for Radiologic Image Research
Department of Radiology, The University of Chicago
5841 South Maryland Avenue, Chicago, Illinois 60637

Abstract

In this study, we developed an optimal filter which maximizes the perceived SNR based on a statistical decision theory model for a human observer. This filter serves as a prewhitening filter that compensates for both the image noise Wiener spectrum and the observer's visual system response, thus allowing the observer to perform matched-filtering in a white noise background during signal detection. However, we found that the filtered image has to be displayed with a strong contrast enhancement factor in order to reduce the effects of observer's internal noise and the display system noise. The use of a large windowing factor results in an image exceeding the dynamic renge of a display system. Due to this limitation, it appears to be difficult to implement the optimal statistical filter (OSF) effectively in a practical digital radiographic imaging system. Therefore, we examined alternative filters by using series approximation of the OSF. The perceived SNR's of the filtered images predicted by the statistical decision theory model indicate that these filters in combination with a moderate windowing factor can improve the detectability of signals over that achieved by the windowing technique alone. We discuss the theoretical basis for the development of these new filters and the results of our calculations. Examples of simple test object images processed by the filters are shown. The potential usefulness and limitations of the various image processing methods in practical settings are discussed.

Introduction

In digital radiography, image processing techniques are often applied to the digital image data so as to enhance the visibility of diagnostic details in the displayed image. Commonly used techniques include overall contrast enhancement (or "windowing"), spatial filtering, and histogram equalization. In recent studies, Ishida et al.[1], Loo et al.[2], and Chan et al.[3] have shown that the detectability of low-contrast objects superimposed on radiographic noisy background can be improved by spatial filtering with unsharp mask filters, Metz filters, or matched filters; by windowing alone; or by windowing in combination with spatial filtering. However, the improvements in detectability achieved by these techniques are limited, and the resulting detectabilities are still far below the upper bounds for an ideal observer that are predicted by statistical decision theory. These results indicate that image processing techniques must be developed to enhance signals and to suppress noise in a way that will compensate for the non-ideal visual detection process of a human observer.

In this study, we attempted to develop an optimal spatial filter for the maximization of a perceived signal-to-noise ratio that is based on a statistical decision theory model for the human observer. The performance of the filter in the presence of internal noise of the human eye-brain system — and limitations on its implementation in a display system with finite dynamic range — will be discussed. Based on the optimal filters, we also developed alternative filters with a series approximation which can improve signal detectabilities beyond those achieved by contrast enhancement and/or the filters studied previously. The characteristics and performance of these new filters have been investigated.

The signal-to-noise ratio model

In recent years, statistical decision theory has been suggested as a viable model for the human visual detection process.[4-7] In the simple task of deciding between the presence or absence of a signal, it has been shown that an optimal decision strategy is to compute a likelihood ratio, which is then compared with an arbitrary threshold value used as a decision criterion.[4] Then, under rather general conditions, the performance of an idealized detector that uses this optimal strategy is determined only by a signal-to-noise ratio (SNR), which can be expressed in terms of the physical characteristics of the image. For the case of a signal superimposed on spatially-correlated (colored) Gaussian noise, such as radiographic mottle, the probability of correctly detecting a signal by an optimal strategy is related to the SNR[5] given by

$$SNR^2_{max} = \int\int_{-\infty}^{\infty} \frac{S^2(\vec{u})}{W(\vec{u})}\, d\vec{u} \qquad (1)$$

where $\vec{u}$ denotes a vector in the two-dimensional spatial frequency space, $S(\vec{u})$ is the Fourier spectrum of the signal, and $W(\vec{u})$ is the noise Wiener spectrum of the imaging system. This SNR may thus be regarded as a performance measure for an ideal detector that employs a decision strategy based on statistical decision theory, and hence it represents an upper bound on actual detection performance.

Evidence exists to suggest that a human observer cannot take into account the effect of colored noise in signal detection tasks, however. By assuming that the human observer is "unaware" of noise coloration and uses a strategy that is optimal for white noise, Wagner[6] showed that human observer performance should be described by a SNR given by

$$SNR_o^2 = \frac{\iint_{-\infty}^{\infty} S^2(\vec{u})\,d\vec{u}}{\left\{\frac{\iint_{-\infty}^{\infty} W(\vec{u})\,S^2(\vec{u})\,d\vec{u}}{\iint_{-\infty}^{\infty} S^2(\vec{u})\,d\vec{u}}\right\}} \quad . \tag{2}$$

Eq. (2) can be interpreted as an SNR for which both the signal and the noise are seen through a sampling aperture with the same spatial profile as the signal to be detected. This model suggests that the statistical decision maker attempts to perform a "matched" filter operation on the image, but fails to "prewhiten" the colored noise. This expression for SNR was subsequently modified by Loo et al. [2] for a human observer to take into account the transfer characteristics of the observer's visual system, which are described by a visual spatial frequency response function (VRF). Furthermore, various studies [1,8-11] have shown that the detectability of low-contrast signals is degraded by an internal noise component of the observer's eye-brain system, which causes fluctuations in the response of the human observer during the signal detection and decision-making processes. Based on their results from digital image processing with a windowing technique, Ishida et al.[1] proposed that the internal noise is statistically independent from the perceived image noise and that its magnitude does not depend on the image noise level. The perceived SNR — which includes the spatial frequency response and the internal noise of the human eye-brain system in combination with his inability to account for noise coloration — is thus given by

$$SNR_I^2 = \frac{\iint_{-\infty}^{\infty} S^2(\vec{u})\,VRF^2(\vec{u})\,d\vec{u}}{\frac{\iint_{-\infty}^{\infty}\left(W(\vec{u})\,VRF^2(\vec{u})\right)\left(S^2(\vec{u})\,VRF^2(\vec{u})\right)d\vec{u}}{\iint_{-\infty}^{\infty} S^2(\vec{u})\,VRF^2(\vec{u})\,d\vec{u}} + N_I^2} \quad , \tag{3}$$

where N_I is the internal noise.

In a digital radiographic system, the noise Wiener spectrum of the displayed image is composed of the noise of the recording system, $W_R(\vec{u})$, and that of the display system, $W_F(\vec{u})$. Furthermore, if image processing such as windowing and linear spatial filtering is applied to the digital image data, both the signal spectrum and the Wiener spectrum of the recording system will be altered before display, whereas the Wiener spectrum of the display system and the internal noise will remain unaffected. Therefore, the perceived SNR of the processed image is given by

$$SNR_p = \frac{\gamma S_p}{\sqrt{\gamma^2 N_R^2 + N_F^2 + N_I^2}} = \frac{S_p}{\sqrt{N_R^2 + \frac{1}{\gamma^2}\left(N_F^2 + N_I^2\right)}} \quad , \tag{4}$$

where

$$S_p = \left\{\iint_{-\infty}^{\infty} S^2(\vec{u})\,|F(\vec{u})|^2 VRF^2(\vec{u})\,d\vec{u}\right\}^{\frac{1}{2}} \quad ; \tag{5}$$

$$N_R = \frac{\left\{\iint_{-\infty}^{\infty}\left(W_R(\vec{u})\,|F(\vec{u})|^2 VRF^2(\vec{u})\right)\left(S^2(\vec{u})\,|F(\vec{u})|^2 VRF^2(\vec{u})\right)d\vec{u}\right\}^{\frac{1}{2}}}{S_p} \quad ; \tag{6}$$

$$N_F = \frac{\left\{\iint_{-\infty}^{\infty}\left(W_F(\vec{u})\,VRF^2(\vec{u})\right)\left(S^2(\vec{u})\gamma\,|F(\vec{u})|^2 VRF^2(\vec{u})\right)d\vec{u}\right\}^{\frac{1}{2}}}{S_p} \quad ; \tag{7}$$

γ is the contrast enhancement factor; and $|F(\vec{u})|$ is the modulation transfer function (MTF) of the filter.

The perceived SNR model in Eq. (4) has been used successfully to explain the improvement in detectability of simple low-contrast objects that can be achieved by digital image processing techniques such as windowing, unsharp mask filtering, Metz filtering, matched filtering, and the effect of pixel size on SNR and threshold contrast.[1-3,12,13] In this study, we developed an optimal filter based on the perceived statistical decision theory model and used the related SNR to predict the efficacy of various image processing techniques.

The optimal statistical filter

Filter MTF

If the SNR derived from the perceived statistical decision theory model adequately predicts human observer performance in a simple detection task, then one can expect that a filter that maximizes this perceived SNR should be the optimal filter for signal processing. From Eq. (4), it can be seen that when a large windowing factor is applied to the image data, the noise of the display system and the observer's internal noise become negligible in comparison to the noise of the recording system, which is contrast-enhanced by the same factor γ as is the signal. Effectively, the SNR of the perceived

image becomes

$$SNR_{p,\gamma\to\infty} = \frac{S_p}{N_R} \quad , \tag{8}$$

or

$$SNR^2_{p,\gamma\to\infty} = \frac{\{\int\int_{-\infty}^{\infty} S^2(\vec{u})\,|F(\vec{u})|^2 VRF^2(\vec{u})\,d\vec{u}\}^2}{\int\int_{-\infty}^{\infty} W_R(\vec{u})\,S^2(\vec{u})\,|F(\vec{u})|^4 VRF^4(\vec{u})\,d\vec{u}} \quad . \tag{9}$$

Applying Schwarz-Buniakowski's inequality, namely,

$$\{\int\int_{-\infty}^{\infty} A(\vec{u})B(\vec{u})\,d\vec{u}\}^2 \le \{\int\int_{-\infty}^{\infty} A^2(\vec{u})\,d\vec{u}\}\{\int\int_{-\infty}^{\infty} B^2(\vec{u})\,d\vec{u}\}, \tag{10}$$

where $A(\vec{u})$ and $B(\vec{u})$ are real and integrable functions, to Eq. (9), one obtains

$$SNR^2_{p,\gamma\to\infty} \le \int\int_{-\infty}^{\infty} \frac{S^2(\vec{u})}{W_R(\vec{u})} d\vec{u} \tag{11}$$

The equality holds if and only if

$$\frac{S(\vec{u})}{\sqrt{W_R(\vec{u})}} = k^2 \sqrt{W_R(\vec{u})}\; S(\vec{u})\,|F(\vec{u})|^2 VRF^2(\vec{u}) \tag{12}$$

where k is an arbitrary constant. Hence, assuming that no zero exists in the VRF $(\vec{u})$ or $W_R(\vec{u})$ and that they are both real functions, a filter of the form

$$F(\vec{u}) = \frac{k}{VRF(\vec{u})\sqrt{W_R(\vec{u})}} \tag{13}$$

should produce a maximum perceived SNR given by

$$SNR^2_{p,max} = \int\int_{-\infty}^{\infty} \frac{S^2(\vec{u})}{W_R(\vec{u})}\, d\vec{u} \quad , \tag{14}$$

which is also the theoretical maximum SNR predicted by statistical decision theory for a detector using the optimal strategy (Eq. (1)). We shall refer to the filter shown in Eq. (13) as the optimal statistical filter (OSF). It is important to note, however, that this filter is optimal only if the observer's internal noise and display system noise are made negligible relative to the filtered noise of the recording system, which may be accomplished by using strong windowing techniques.

The OSF depends on the VRF of the observer and the frequency spectrum of the colored noise, but is independent of the signal spectrum. This occurs because the perceived SNR is derived for a statistical decision-maker that can "match-filter" the image but cannot "whiten" the perceived noise. Therefore, a filter that prewhitens the perceived noise by compensating for the colored input noise and the band-pass effects of the observer VRF, in combination with the observer's internal "matched-filtering" decision process, will result in the optimal detection strategy expected by statistical decision theory.

Effect of the optimal statistical filter

In our study, test object images were produced by superimposing low-contrast square patterns of uniform density on digitized uniform noisy radiographic backgrounds. The signal spectrum is therefore represented by the two-dimensional sinc function:

$$S(\vec{u}) = L^2 \Delta D\, \mathrm{sinc}(\pi u_x L)\, \mathrm{sinc}(\pi u_y L) \quad , \tag{15}$$

where ΔD is the object contrast in optical density units and L is the length of one side of the square. We employed a conventional screen-film system, Kodak X-Omatic Regular/XRP, as the x-ray receptor, and digital images were reconstituted on a Fuji "scanner" film for display.[14] The noise Wiener spectra of these systems were measured by an analog electronic Fourier analysis method. The visual response function used[15] depends on the viewing distance. We assumed a viewing distance of 50 cm in this study. The VRF was measured for spatial frequencies above about 0.06 cycle/mm. We obtained the VRF values below this frequency by extrapolation from the experimental data, and the VRF at zero frequency was assumed to be zero. The Wiener spectra of our image recording and display systems, and the VRF were

shown in our previous paper.[3] The internal noise, N_I, for a human observer in this simple detection task was estimated [1] to be 0.0033 optical density units, which corresponds to approximately 80% of the perceived noise content of radiographic mottle in the X-Omatic Regular/XRP system.

Based on Eqs. (3) or (4), and (15), it follows that the SNR is proportional to the contrast of the signal, ΔD, if the filter MTF does not depend on ΔD. Thus, the threshold contrast of the original image, ΔD_t, required for a given detection accuracy can be derived from knowledge of the corresponding threshold SNR, SNR_t:

$$\Delta D_t = \left(\frac{\Delta D}{SNR}\right) SNR_t \quad . \tag{16}$$

The ratio $(\Delta D/SNR)$ can be calculated from Eqs. (4) and (15) for given imaging and viewing conditions. For simple radiologic objects superimposed on a uniform noisy background, Ishida et al. [11] and Ohara et al. [12] determined that a constant SNR of 3.8 was required for 50% detection accuracy in 18-alternative forced-choice (AFC) experiments. Therefore, to predict threshold contrasts, we assumed that SNR_t was equal to 3.8.

In our calculations, the signal and noise contents were obtained by numerical integration of the corresponding spectra. Since the image recorded on the radiograph was digitized with a sampling distance of 0.1 mm, the Nyquist frequency occurs at 5 cycles/mm, [16] which was taken as the cut-off frequency in the numerical integration in both the x- and y-directions.

Fig. 1 shows the contrast-detail (C-D) curve predicted for the original and processed images by use of Eq.(16). The SNRs of the original images and those with windowing alone were calculated from Eq.(3) and Eq.(4), respectively, whereas those with the OSF was calculated from Eq.(14). Thus, the OSF curve indicates the theoretical minimum threshold contrasts required for the detection of these signals with 50% accuracy in 18-AFC experiments. We show here images processed with a windowing technique using $\gamma=4$; however, threshold contrasts predicted at $\gamma=\infty$ are only about 3% lower than those at $\gamma=4$. Clearly, the predicted improvement in detectability obtained with the windowing technique is far less than that predicted with the OSF.

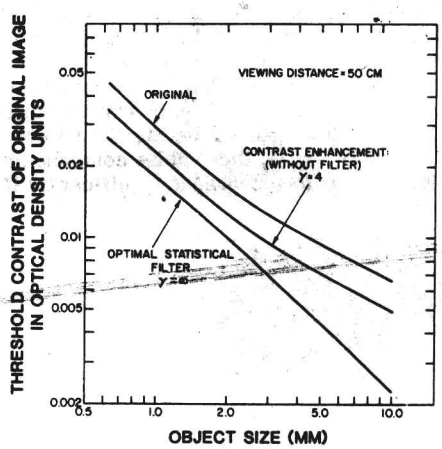

Fig 1. Predicted contrast-detail curves for the original images and images processed by the optimal statistical filter and/or windowing techniques.

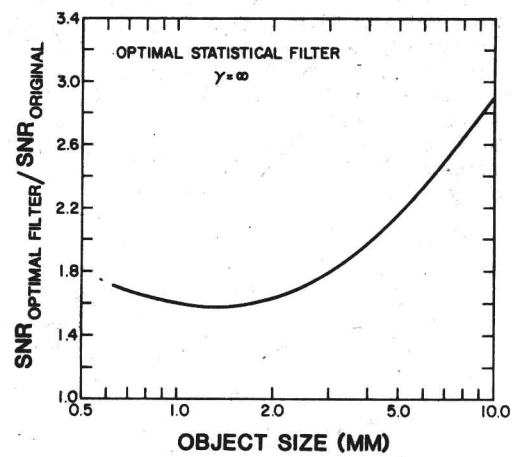

Fig. 2. Dependence of the SNR ratio on object size for images processed with the OSF.

The improvement in the perceived SNR achieved by image processing is evaluated by the ratio $SNR_{processed}/SNR_{original}$, which will be referred to as the "SNR ratio" in the following discussion. Fig. 2 shows the dependence of the SNR ratio on object size for the images processed with the OSF. The perceived SNR can be increased by a factor of about 1.6 to 2.9 from that of the original image, depending on the object size.

The perceived SNRs for the OSF just described were calculated based on Eq. (14), which implies that both the VRF and the radiographic noise Wiener spectrum are exactly compensated for in the perceived image. To implement the OSF in an image processing algorithm, however, the filter MTF becomes infinite if the VRF approaches zero. For the VRF described previously, we assumed its value to be a finite constant from 0 to 0.01 cycle/mm for the calculation of the filter MTF. Fig. 3 shows the resulting MTF of the OSF, which prewhitens the perceived noise of the X-Omatic Regular/XRP system at a viewing distance of 50 cm. Since both $VRF(\vec{u})$ and $W_R(\vec{u})$ are assumed to be rotationally symmetric, only a cross section of $MTF(\vec{u})$ is plotted. The constant k in Eq. (13) was chosen to be $VRF(0)\sqrt{W_R(0)}$, so that F(0)=1 and the background level of the filtered image is made equal to that of the original image.

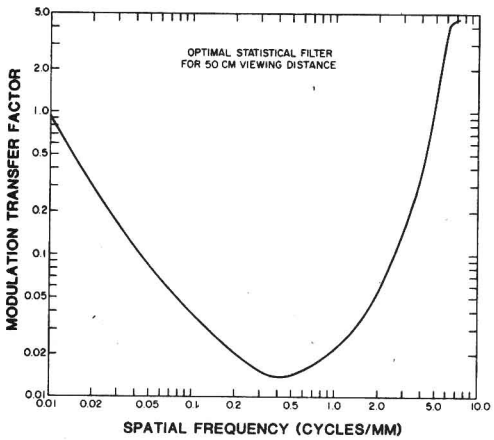

Fig. 3. Modulation transfer factor of the optimal statistical filter.

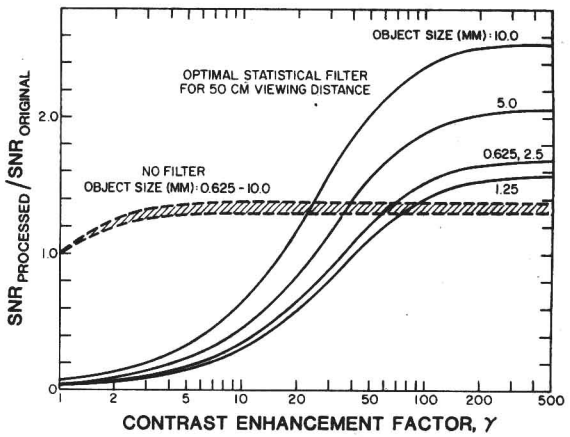

Fig. 4. Dependence of the SNR ratio on contrast enhancement factor for images processed with the OSF.

The perceived SNR of an image filtered by the OTF shown in Fig. 3 was calculated as a function of γ by using Eq. (4). Fig. 4 illustrates the relationship between the SNR ratio and γ. It is apparent that the filter actually degrades the perceived SNR at small γ values. Substantial gain in SNR over that obtained by windowing alone occurs only when γexceeds a value of 20 to 100, depending on the object size. The degradation of the SNR at small γ values can be explained by the presence of the internal noise and the display system noise. When the OSF -- which was derived for large γ -- is applied to the image, both the signal content, S_D, and the radiographic noise content, N_R, are suppressed substantially. The ratio of S_D/N_R increases, however. Without windowing, the internal noise and the display system noise become the predominant noise components in the perceived noise, as shown in Fig. 5. If windowing is applied to the filtered image, N_I and N_F are effectively reduced by a factor of $1/\gamma$ compared to N_R. As seen in Fig. 5, these noise components can be considered negligible only when γ is larger than about 200. The perceived SNR is therefore degraded significantly if strong windowing is not employed in combination with the "optimal" statistical filter.

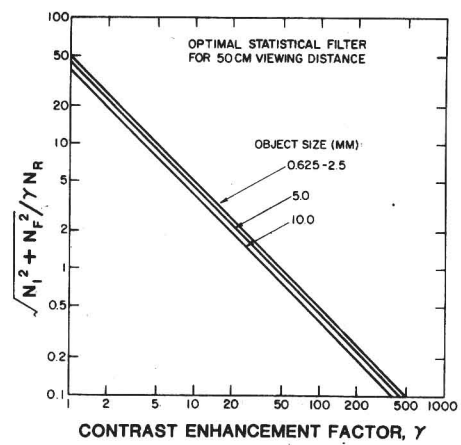

Fig. 5. Dependence of the internal noise plus film noise relative to the radiographic noise on contrast enhancement factor.

It may also be noted that the asymptotic values of the SNR ratios at infinite γ values do not approach those shown in Fig. 2, especially for large object sizes. This discrepancy indicates the fact that if the "true" VRF contains zero values, the OSF implemented with a finite upper bound on its MTF will not be able to compensate for the lost frequency content at those zeros.

Application of the optimal statistical filter to radiographic images

Our test object images were prepared in a way described in detail previously.[3] Briefly, a Fuji drum scanner/computer system was employed for digitization of radiographs and for output of a digital image on film. A uniformly exposed film sample of radiographic noise was digitized with a 0.1 mm x 0.1 mm aperture, 10 pixels/mm sampling rate, and 1024 grey levels within the density range of 0.2 to 2.75. The signals were produced by digitally superimposing square patterns of various sizes and contrasts on the noise sample at predetermined locations.

From the "original" digitized image containing the square objects, we prepared "processed" images by manipulation of the digital data. For the filtering techniques, the original image containing 1024 x 1024 pixels was Fourier-transformed by an FFT algorithm into the spatial frequency domain. The Fourier spectrum of the image was multiplied by the MTF of the filter and then inversely Fourier-transformed back to the spatial domain. The filtered image can be further enhanced by subsequent use of the contrast enhancement technique, which is accomplished by increasing the grey level variation of the image data by a factor equal to the contrast enhancement factor. The average pixel value of the processed image was maintained at that of the unprocessed image by shifting the grey levels linearly.

Fig. 6(a)-(d) show an original image and three processed images containing objects of sizes 5 mm, 2.5 mm, and 1.25 mm at four contrast levels. The three processed images were obtained from a single filtered image that was displayed with windowing factors of 1, 20, and 100, respectively. It can be seen that the filtered image with γ=1 has very low SNR compared with the original image. As γ increases to 20, the square patterns appear to become more conspicuous. However, perhaps surprisingly, the visibility of the square patterns is not improved further when γ is increased from 20 to 100, as would be expected from the predicted SNR ratios shown in Fig. 4. These unexpected results have been analyzed theoretically[17] and will be reported elsewhere. We shall describe briefly in the following the cause of this phenomenon, which limits the usefulness of the OSF.

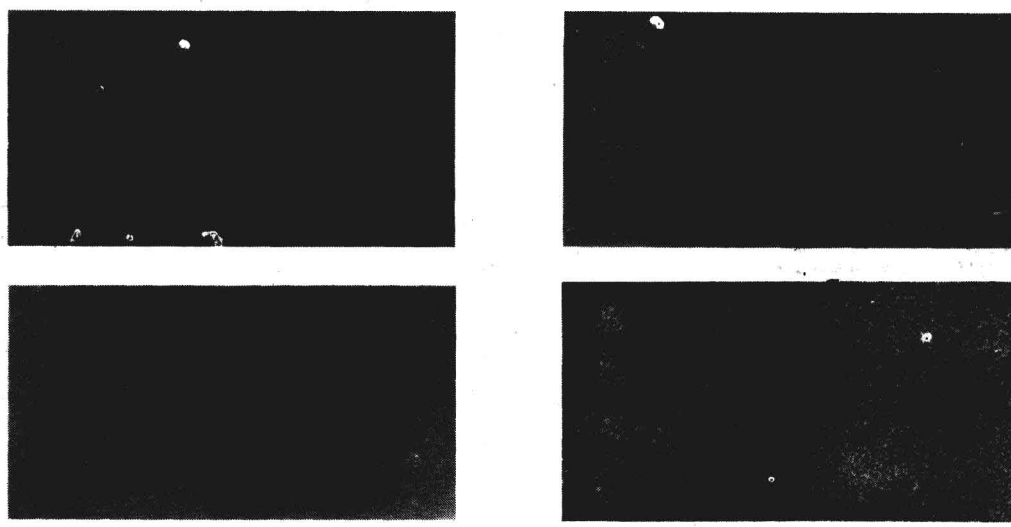

Fig. 6. Test object images: (a) original, and processed with the optimal statistical filter in combination with (b) γ=1, (c) γ=20, (d) γ=100.

Effect of finite display range on windowing technique

The expression for the perceived SNR (Eq. (4)) was derived for images displayed on an idealized analog system, without taking into consideration the effect of the finite range of displayed pixel values that can be achieved with a real digital imaging system. Schematically shown in Fig. 7(a) - (c) are histograms of pixel values in an image that consists of a signal with constant contrast superimposed on a uniform background of Gaussian noise. The pixel values are normalized to a display range of unity. The pixel values fall well within the display range when no windowing is applied (Fig. 7(a)). With a moderate γvalue such that the Gaussian distributions of pixel values are essentially undistorted by the windowing, the signal contrast increases in proportion to γ (Fig. 7(b)). However, if γ is increased further, the fractions of pixels which reach the maximum or minimum values in the display scale increase rapidly. The difference in the average pixel values in the signal region and in the noise region begins to decrease, due to the pile-up of pixel values in both regions at the maximum or minimum of the display range. When γ is very large as shown in Fig. 7(c), the fraction of pixels with intermediate values becomes negligibly small, and any further increase in γ will not change the signal contrast.

The effect of finite display range on the displayed signal contrast after windowing depends on a variety of parameters such as the noise level, window center, display center, the displayed means of the noise and signal plus noise distributions, relative to the display range, as well as the relationship between pixel values and displayed brightness or optical density. Despite the complicated mathematical expressions,[17] the general trends of the dependence of the signal contrast on γ for a variety of conditions can be illustrated by the curves shown in Fig. 8. We assumed here that the pixel values were linearly related to optical density and that the effective density after windowing was derived from the average light transmission. The displayed signal contrast is normalized to its value at infinite γ. In general, the signal contrast increases in proportion to γ at small γ, reaches a maximum, decreases, and then levels off at large γ. The γvalue corresponding to the maximum signal contrast decreases with increasing noise level. Our results indicate that, typically, a γ value larger than 10 to 50 should not be employed for radiographic images.

Based on these findings and the results shown in Fig. 5, it can be seen that the performance of the OSF is limited by the finite dynamic range of a display system. This is because the observer's internal noise plus the film noise is larger than or comparable to the perceived filtered radiographic noise when γ values are less than 50.

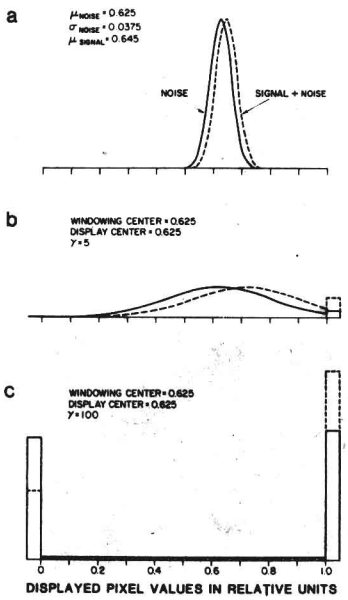

Fig. 7. Schematic diagram of histograms of the pixel values for a signal of constant contrast superimposed on a uniform background with Gaussian noise. μ_{noise} is the mean and σ_{noise} is the standard deviation of the noise distribution. μ_{signal} is the mean of the signal and noise distribution (a) γ =1, (b) γ =5, and (c) γ =100.

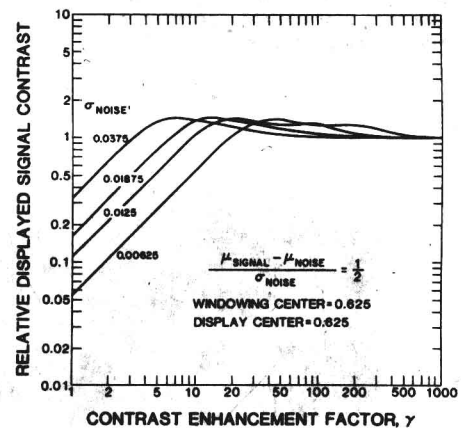

Fig. 8. Dependence of the relative displayed signal contrast on contrast enhancement factor for images with Gaussian noise of various standard deviations.

Optimal statistical filter with a series approximation

In an effort to obtain a filter which has frequency characteristics similar to the OSF but requires only a moderate windowing factor, we applied a series approximation method to the OSF. The n^{th} order series approximation of the OSF is given by

$$F_n(u) = \frac{1}{n+1} \sum_{i=0}^{n} \left\{1 - \frac{VRF(u)\sqrt{W_R(u)}}{(VRF(u)\sqrt{W_R(u)})_{max}}\right\}^i , \qquad (17)$$

where u is spatial frequency in the radial direction, and the subscript "max" denotes the maximum value of $VRF(u)\sqrt{W_R(u)}$. Furthermore, we employed an analytical approximation of the VRF:

$$VRF(u) = \exp\left\{ - \frac{(\ln u - \ln(25u_o/D))^2}{2\,(0.973)^2} \right\} , \qquad (18)$$

which is a Gaussian curve on a logarithmic frequency scale. The constant u_o is the spatial frequency at which the VRF at a viewing distance of 25 cm is a maximum; u_o can be regarded as 1 cycle/mm for the experimental VRF data that we chose. D is the viewing distance in cm at which the VRF is to be calculated. Fig. 9 compares the experimental VRF and the analytical approximation at a viewing distance of 25 cm. It may be noted that the VRF for different viewing distances can be obtained simply by shifting laterally the curve shown by a factor of 25/D.

Fig. 10 shows the MTFs of the series approximation filters with various orders. The minimum of the MTF for a filter of order n is equal to 1/(n + 1), which occurs at $VRF(u)\sqrt{W_R(u)} = \left[VRF(u)\sqrt{W_R(u)} \right]_{max}$. The filter with n=70 is a close approximation of the OSF shown in Fig. 3 in the frequency range from about 0.1 to 4 cycles/mm. Above 4 cycles/mm, the OSF rises to much higher MTF values than the series approximation.

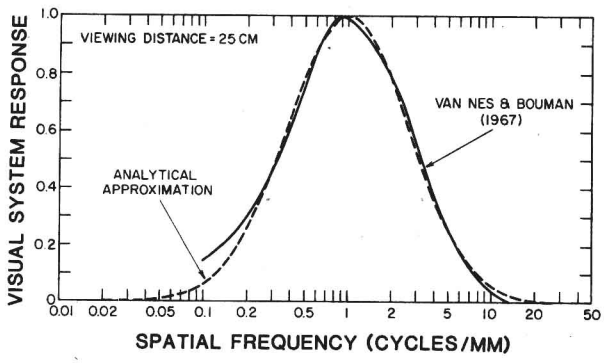

Fig. 9. Comparison of the experimental VRF [15] at 25 cm viewing distance with the analytical approximation.

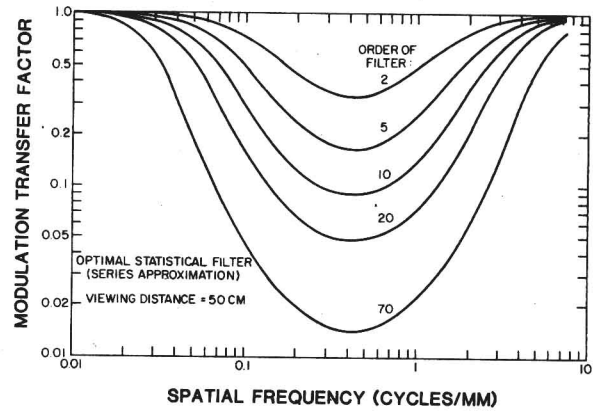

Fig. 10. Modulation transfer factors of the series approximation of the OSF with various orders.

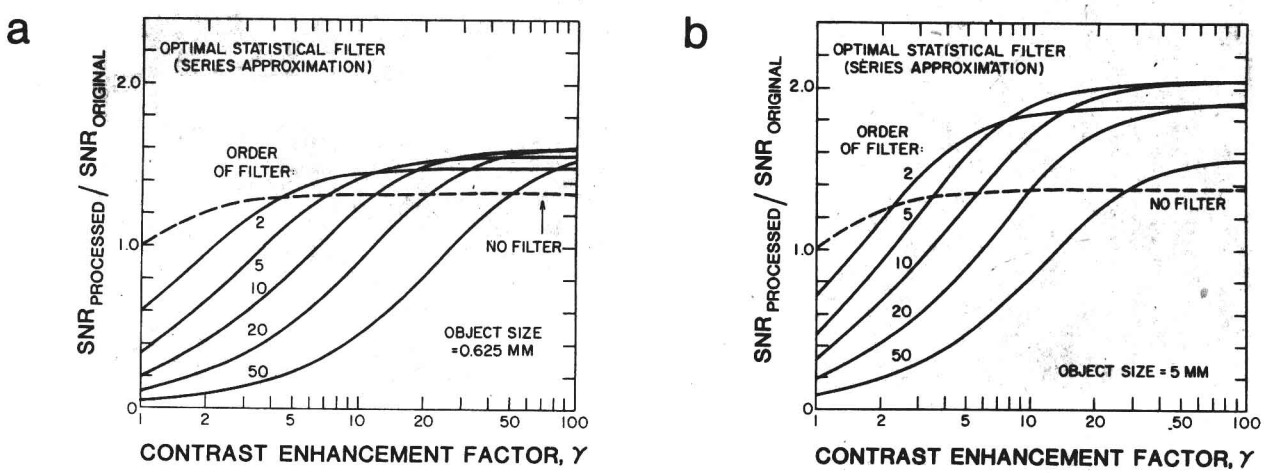

Fig. 11. Dependence of the SNR ratio on contrast enhancement factor for images processed with the series approximation of the OSF. Object sizes: (a) 0.625mm, (b) 5mm.

Effect of the optimal statistical filter (series approximation)

The SNR ratios obtained by using the series approximation filters were calculated from Eqs. (3) and (4) as a function of γ and are shown in Fig. 11(a) - (b). For a given object size, the SNR ratio increases less rapidly with a higher-order filter than with a lower-order filter as γ increases; a higher-order filter yields a higher asymptotic SNR ratio at large windowing factors, however. The trend of the curves for the high-order filters is similar to those for the OSF (Fig. 4), as expected. The filter with n=2 can achieve SNR ratios higher than those achieved by windowing alone for γ values above about 5. This is because the radiographic noise content is not suppressed as much by the series approximation filter as by the OSF. Consequently, the internal noise and the display system noise can be neglected at a moderate value of γ. Thus, this filter appears to be a practical alternative to the OSF.

Fig. 12 shows the C-D curve predicted for 50% detection accuracy in 18-AFC experiments with images processed using the n=2 series approximation filter in combination with γ=10 windowing. The improvement in the detectability of the objects exceeds that achieved by windowing alone, although the threshold contrasts remain higher than the theoretical minimum values.

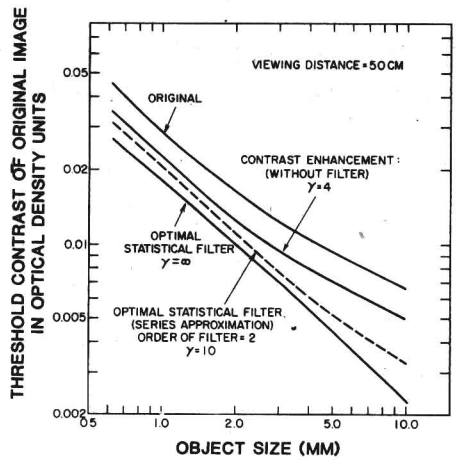

Fig. 12. Comparison of the predicted contrast-detail curve for images processed with the series approximation of the OSF (n=2, γ=10) with curves for the original images and images processed with other techmiques.

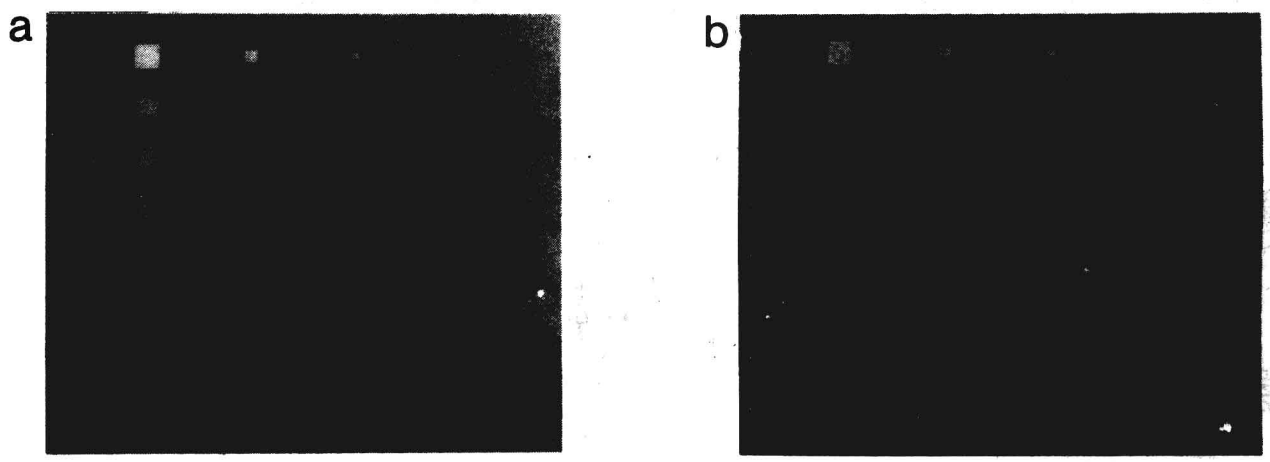

Fig. 13. Test object images processed with (a) the series approximation of the OSF (n=2, γ=10), and (b) contrast enhancement technique (γ=4) alone.

Application of the optimal statistical filter (series approximation) to radiographic images

We applied the n=2 filter to the test object radiographs described previously. Fig. 13 compares an image processed using this filter with γ=10 and an image processed with γ=4 windowing alone. Note that the region shown here includes square patterns with original contrasts lower than those shown in Fig. 6(a). The image processed with the n=2 filter appears to have less quantum mottle than that processed with windowing alone; this can probably be attributed to the filter's relative suppression of noise content in the mid-frequency range. In addition, the filter causes edge sharpening due to its enhancement of the high frequency content of the image. The enhancement of the low frequency content of the image, on the other hand, results in the improved visibility of some low-contrast large patterns in the background, which are almost invisible in the original and the windowed-only images. Therefore, this filter may be useful for processing radiographs that contain both low-contrast large lesions and subtle abnormalities. Observer performance experiments are underway to evaluate the effectiveness of these series approximation filters in comparison to other image processing techniques, and their usefulness in processing clinical images will be investigated in the future.